

Surface doping manipulation of the insulating ground states in $Ta_2Pd_3Te_5$ and $Ta_2Ni_3Te_5$

Bei Jiang(江北), Jingyu Yao(姚静宇), Dayu Yan(闫大禹), Zhaopeng Guo(郭照芃), Gexing Qu(屈歌星), Xiutong Deng(邓修同), Yaobo Huang(黄耀波), Hong Ding(丁洪), Youguo Shi(石友国), Zhijun Wang(王志俊), and Tian Qian(钱天)

Citation: Chin. Phys. B, 2024, 33 (**6**): 067402. DOI: 10.1088/1674-1056/ad362e
Journal homepage: http://cpb.iphy.ac.cn; http://iopscience.iop.org/cpb

What follows is a list of articles you may be interested in

Electronic structure and effective mass of pristine and Cl-doped $CsPbBr_3$

Zhiyuan Wei(魏志远), Yu-Hao Wei(魏愉昊), Shendong Xu(徐申东), Shuting Peng(彭舒婷), Makoto Hashimoto, Donghui Lu(路东辉), Xu Pan(潘旭), Min-Quan Kuang(匡泯泉), Zhengguo Xiao(肖正国), and Junfeng He(何俊峰)
Chin. Phys. B, 2024, 33 (**5**): 057403. DOI: 10.1088/1674-1056/ad3c31

Distinct behavior of electronic structure under uniaxial strain in $BaFe_2As_2$

Jiajun Li(李佳俊), Giao Ngoc Phan, Xingyu Wang(王兴玉), Fazhi Yang(杨发枝), Quanxin Hu(胡全欣), Ke Jia(贾可), Jin Zhao(赵金), Wenyao Liu(刘文尧), Renjie Zhang(张任杰), Youguo Shi(石友国), Shiliang Li(李世亮), Tian Qian(钱天), and Hong Ding(丁洪)
Chin. Phys. B, 2024, 33 (**1**): 017401. DOI: 10.1088/1674-1056/acd8af

Rubidium-induced phase transitions among metallic, band-insulating, Mott-insulating phases in 1*T*-TaS_2

Zhengguo Wang(王政国), Weiliang Yao(姚伟良), Yudi Wang(王宇迪), Ziming Xin(信子鸣), Tingting Han(韩婷婷), Lei Chen(陈磊), Yi Ou(欧仪), Yu Zhu(朱玉), Cong Cai(蔡淙), Yuan Li(李源), and Yan Zhang(张焱)
Chin. Phys. B, 2023, 32 (**10**): 107404. DOI: 10.1088/1674-1056/acec40

Conservation of the particle-hole symmetry in the pseudogap state in optimally-doped $Bi_2Sr_2CuO_{6+\delta}$ superconductor

Hongtao Yan(闫宏涛), Qiang Gao(高强), Chunyao Song(宋春尧), Chaohui Yin(殷超辉), Yiwen Chen(陈逸雯), Fengfeng Zhang(张丰丰), Feng Yang(杨峰), Shenjin Zhang(张申金), Qinjun Peng(彭钦军), Guodong Liu(刘国东), Lin Zhao(赵林), Zuyan Xu(许祖彦), and X. J. Zhou(周兴江)
Chin. Phys. B, 2022, 31 (**8**): 087401. DOI: 10.1088/1674-1056/ac7214

Measurement of electronic structure in van der Waals ferromagnet $Fe_{5-x}GeTe_2$

Kui Huang(黄逵), Zhenxian Li(李政贤), Deping Guo(郭的坪), Haifeng Yang(杨海峰), Yiwei Li(李一苇),Aiji Liang(梁爱基), Fan Wu(吴凡), Lixuan Xu(徐丽璇), Lexian Yang(杨乐仙), Wei Ji(季威),Yanfeng Guo(郭艳峰), Yulin Chen(陈宇林), and Zhongkai Liu(柳仲楷)
Chin. Phys. B, 2022, 31 (**5**): 057404. DOI: 10.1088/1674-1056/ac5c3c

---

RAPID COMMUNICATION

Surface doping manipulation of the insulating ground states in $Ta_2Pd_3Te_5$ and $Ta_2Ni_3Te_5$

Bei Jiang(江北)[1,2,†], Jingyu Yao(姚静宇)[1,2,†], Dayu Yan(闫大禹)[1,2,†], Zhaopeng Guo(郭照芃)[1], Gexing Qu(屈歌星)[1,2], Xiutong Deng(邓修同)[1,2], Yaobo Huang(黄耀波)[4], Hong Ding(丁洪)[5,6], Youguo Shi(石友国)[1,2,3], Zhijun Wang(王志俊)[1,2], and Tian Qian(钱天)[1,‡]

[1] *Beijing National Laboratory for Condensed Matter Physics and Institute of Physics, Chinese Academy of Sciences, Beijing* 100190, *China*
[2] *University of Chinese Academy of Sciences, Beijing* 100049, *China*
[3] *Songshan Lake Materials Laboratory, Dongguan* 523808, *China*
[4] *Shanghai Synchrotron Radiation Facility, Shanghai Advanced Research Institute, Chinese Academy of Sciences, Shanghai* 201204, *China*
[5] *Tsung-Dao Lee Institute, New Cornerstone Science Laboratory, and School of Physics and Astronomy, Shanghai Jiao Tong University, Shanghai* 201210, *China*
[6] *Hefei National Laboratory, Hefei* 230088, *China*

(Received 20 February 2024; revised manuscript received 12 March 2024; accepted manuscript online 21 March 2024)

Manipulating emergent quantum phenomena is a key issue for understanding the underlying physics and contributing to possible applications. Here we study the evolution of insulating ground states of $Ta_2Pd_3Te_5$ and $Ta_2Ni_3Te_5$ under *in-situ* surface potassium deposition via angle-resolved photoemission spectroscopy. Our results confirm the excitonic insulator character of $Ta_2Pd_3Te_5$. Upon surface doping, the size of its global gap decreases obviously. After a deposition time of more than 7 min, the potassium atoms induce a metal–insulator phase transition and make the system recover to a normal state. In contrast, our results show that the isostructural compound $Ta_2Ni_3Te_5$ is a conventional insulator. The size of its global gap decreases upon surface doping, but persists positive throughout the doping process. Our results not only confirm the excitonic origin of the band gap in $Ta_2Pd_3Te_5$, but also offer an effective method for designing functional quantum devices in the future.

Keywords: excitonic insulator, metal–insulator phase transition, surface doping, angle-resolved photoemission spectroscopy

PACS: 74.25.Jb, 79.60.–i, 71.35.–y, 71.30.+h **DOI:** 10.1088/1674-1056/ad362e

1. Introduction

Correlated systems exhibit a range of exotic phenomena due to complex many-body interactions. These include high-temperature superconductivity, charge density wave, heavy fermions, and so on. A profound understanding of these phenomena is crucial in condensed matter physics. Furthermore, manipulating exotic quantum phenomena can establish the basis for designing functional devices. A notable case in this realm is the excitonic insulator (EI), emerging from electron–hole Coulomb interactions. In materials like semiconductors with small bandgap or semi-metals with small band overlap, excitons can spontaneously form and condense at finite temperature, stabilized by the Coulomb interactions between electrons and holes and open a gap around Fermi level (E_F).[1–4] In the scenario of EIs, the insulating ground state is particularly sensitive to the concentration of charge carriers. An increase in charge carriers will effectively enhance the screen effect of the Coulomb interactions and make the excitons unstable,[5–9] as manifested in the reduction of the band gap. If the number of charge carriers is sufficiently large, the system will transform into normal semiconductor/semimetal states. Therefore, carriers doping offers an effective way to manipulate the ground state of EI and induce phase transitions.

To date, only a few intrinsic materials have been proposed as candidates for EI, such as 1*T*-$TiSe_2$[10–16] and Ta_2NiSe_5.[17–23] And their insulating ground states can be significantly manipulated by surface or bulk doping.[5,24–26] Recent studies suggest that a new material, $Ta_2Pd_3Te_5$ might be another EI candidate.[27–29] First-principles calculations show that $Ta_2Pd_3Te_5$ has a semi-metallic band structure with a small band overlap, whereas angle-resolved photoemission spectroscopy (ARPES) and scanning tunneling spectroscopy (STS) measurements reveal an insulating state with a global gap around the Fermi level (E_F) at low temperatures. A closer examination involving the consideration of inter-band electron–hole interactions in theoretical models aligns well with these experimental observations. This alignment suggests that the exciton condensation could be the driving force behind the observed insulating state. Meanwhile, ARPES measurements also provide evidence for gap closing via thermal activation, pump laser pulses or bulk chemical doping, which is also consistent with the EI scenario. In contrast, $Ta_2Ni_3Te_5$, an

[†] These authors contributed equally to this work.
[‡] Corresponding author. E-mail: tqian@iphy.ac.cn

© 2024 Chinese Physical Society and IOP Publishing Ltd

isostructural compound to $Ta_2Pd_3Te_5$ is predicted to be a conventional semiconductor.[30] Consistent with this prediction, ARPES measurements show that the band structure has negligible differences at various temperatures. $Ta_2Pd_3Te_5$ and $Ta_2Ni_3Te_5$ share the same crystal structure with Ni and Pd belonging to the same group in the periodic table. However, they exhibit distinct electronic properties motivating us to investigate their evolution under surface doping.

In this work, we successfully induced a metal–insulator phase transition in $Ta_2Pd_3Te_5$ via surface alkali metal doping, while no such transition occurred in $Ta_2Ni_3Te_5$. Utilizing ARPES, we first confirmed that both $Ta_2Pd_3Te_5$ and $Ta_2Ni_3Te_5$ have an insulating ground state with a global band gap. Upon gradual surface potassium doping, we observed notable shifts of both the conduction band (CB) and valence band (VB) shifted towards higher binding energies in $Ta_2Pd_3Te_5$, resulting in a narrowing of the band gap. In addition to the effects of chemical potential shift, this behavior may be attributed to exciton instability together with the Stark effect. The CB and VB in $Ta_2Pd_3Te_5$ cross with each other at a sufficient potassium dose, resulting in a gapless semi-metallic state. In $Ta_2Ni_3Te_5$, both CB and VB also shift towards higher binding energies upon gradual surface potassium doping. Although the band gap decreases, it persists throughout the doping process. The contrasting responses to surface doping between $Ta_2Pd_3Te_5$ and its isostructural compound $Ta_2Ni_3Te_5$ not only confirm that $Ta_2Pd_3Te_5$ possessed an excitonic insulating ground state, where additional carriers will enhance the screen effect of the Coulomb interactions between electrons and holes, leading the system recover to a normal semimetallic state, while $Ta_2Ni_3Te_5$ is a conventional semiconductor without any exciton condensation. These findings also offer an effective method for manipulating the insulating states or inducing metal–insulator phase transition in $Ta_2Pd_3Te_5$, which could be utilized to design functional quantum devices in the future.

2. Material and methods

High-quality single crystals of $Ta_2Pd_3Te_5$ (or $Ta_2Ni_3Te_5$) were synthesized by a self-flux method. Starting materials of Ta (powder, 99.999%), Pd (or Ni) (bar, 99.9999%) and Te (lump, 99.9999%) were mixed in an Ar-filled glove box at a molar ratio of Ta:Pd (or Ni):Te = 2:4.5:7.5. The mixture was placed in an alumina crucible, which was then sealed in an evacuated quartz tube. The tube was heated to 950 °C over 10 h and dwelt for 2 d. Then, the tube was slowly cooled down to 800 °C at a rate of 0.5 °C/h. Finally, the extra flux was removed by centrifuging at 800 °C. After centrifuging, the black and shiny single crystals of $Ta_2Pd_3Te_5$ (or $Ta_2Ni_3Te_5$) were picked out from the remnants in the crucible.

Laser-based ARPES measurements were performed at the Institute of Physics, Chinese Academy of Sciences using a Scienta Omicron DA30-L analyzer. The photon energy was 6.994 eV, generated by second harmonic generation using a KBBF crystal. The s or p linear polarized mode of the laser could be switched by placing a half-wave plate on the light path or not. The overall energy resolution was ~ 2 meV and the angular resolution was $\sim 0.2^\circ$. Synchrotron ARPES experiments were conducted at the Dreamline beamline at the Shanghai Synchrotron Radiation Facility. The overall energy resolution was ~ 15 meV. The E_F of all experiments was referenced by measuring the Fermi edge of a polycrystalline gold which has been sputtered by Ar ions in advance. All the samples prepared for ARPES were cleaved *in-situ* and measured in an ultrahigh vacuum with a base pressure better than 7×10^{-11} Torr. Surface doping was achieved via potassium deposition conducted *in-situ* using a SAES alkali metal dispenser. The deposition process was repeated multiple times with a working current of 6 A, and the doping level was represented using the total deposition time. For each doping step, the time for ARPES data collection was set to be approximately 25 min and the sample temperature was maintained at 20 K to prevent desorption of potassium adatoms from the sample surface. First-principles calculations were performed within the framework of DFT using the projector augmented wave (PAW) method, as implemented in the Vienna *ab initio* simulation package (VASP). The modified Becke–Johnson (MBJ) functional was selected to describe the exchange potential.

3. Results and discussion

The compound of $Ta_2Pd_3Te_5$ (or $Ta_2Ni_3Te_5$) crystalizes in an orthorhombic crystal structure with the space group *Pnma* (No. 62), the lattice constants are $a = 13.953$ (or 13.866) Å, $b = 3.704$ (or 3.692) Å, and $c = 18.599$ (or 17.689) Å. The crystal structure is shown in Fig. 1(a). Each unit cell consists of two $Ta_2Pd_3Te_5$ (or $Ta_2Ni_3Te_5$) monolayers stack along the a-axis through weak van der Waals forces. Within each monolayer, Ta and Pd (or Ni) form one-dimensional (1D) chains along the b-axis, which are sandwiched by Te layers. The natural cleavage plane is the (100) plane. Figures 1(c) and 1(d) show the density functional theory (DFT) calculated band structure of $Ta_2Pd_3Te_5$ and $Ta_2Ni_3Te_5$, the quasi-1D crystal structure makes the dispersion along Γ–Y most obvious in these two materials. $Ta_2Pd_3Te_5$ exhibits a semi-metallic band structure with a small band overlap of VB and CB, approximately 42 meV, whereas $Ta_2Ni_3Te_5$ displays a semiconductor-like band structure with a global band gap of around 31 meV. In our previous study, $Ta_2Pd_3Te_5$ is proposed to be an EI candidate with a global gap at a temperature below 300 K.[27] Furthermore, as the temperature increases, the CB shifts downwards while the VB shifts upwards, causing an obvious reduction of the band gap. The system eventually evolves into a band structure with nearly zero gap with linear

dispersion at 300 K. In contrast, ARPES experiments demonstrate that $Ta_2Ni_3Te_5$ has a semiconductor-like band structure, which is consistent with the DFT calculation. As the temperature increases, the VB of $Ta_2Ni_3Te_5$ undergoes negligible changes except for thermal broadening.[28] Having drastically different properties while sharing the same structure motivates us to investigate their different evolution under surface alkali metal doping.

First, we examine their band structure. Figure 2 displays intensity plots of ARPES data of $Ta_2Pd_3Te_5$ and $Ta_2Ni_3Te_5$ along $\bar{\Gamma}$–$\bar{Y}$ under different experimental conditions. Due to the limited thermal broadening, the CB is not visible for both $Ta_2Pd_3Te_5$ and $Ta_2Ni_3Te_5$ under s and p polarization at 20 K. At 120 K, the CB is visible for $Ta_2Pd_3Te_5$ after dividing the data with the Fermi–Dirac distribution function under p polarization. However, the CB remains invisible for $Ta_2Ni_3Te_5$ under both s and p polarization at 120 K. In fact, we have tried to visualize the CB of $Ta_2Ni_3Te_5$ by performing experiments at 300 K, but the CB is still invisible. This may be because the CB of $Ta_2Ni_3Te_5$ is relatively far away from E_F, combined with the consequence of a relatively low spectral weight. We believe the DFT calculations in Fig. 1(d) underestimate the gap size of $Ta_2Ni_3Te_5$. However, these data can confirm that both $Ta_2Pd_3Te_5$ and $Ta_2Ni_3Te_5$ have an insulating ground state, which is consistent with previous study. Given that the CB of $Ta_2Pd_3Te_5$ is visible due to the thermal broadening effect, we also test the orbital component of CB via synchrotron-based ARPES at high temperatures. In a non-interacting regime, the CB of $Ta_2Pd_3Te_5$ originates from the Ta-d_{z^2} orbital. Then, it will hybridize with Pd-d_{xz} and Te-p_x orbitals when considering inter-band electron–hole interactions. Therefore, we perform photon energy ($h\nu$)-dependent ARPES measurement at 150 K to test the orbital components of CB. For transition metal compounds, when $h\nu$ is tuned to the binding energies of p orbitals, the spectral intensities of the bands originating from d orbitals will be suppressed due to p–d antiresonance.[31,32] Figure 2(d) displays the $h\nu$ dependence of the spectral intensities at a constant energy of 0.02 eV above E_F at $\bar{\Gamma}$. Except for the significant suppression corresponding to Ta $5p_{3/2}$ and $5p_{1/2}$ orbitals, the spectral intensities also show dip and kink features corresponding to Pd $4p_{3/2}$ and $4p_{1/2}$ orbitals, as indicated by the black arrows. This demonstrates the existence of band hybridization of $Ta_2Pd_3Te_5$ in its insulating state, confirming the excitonic origin of the band gap.

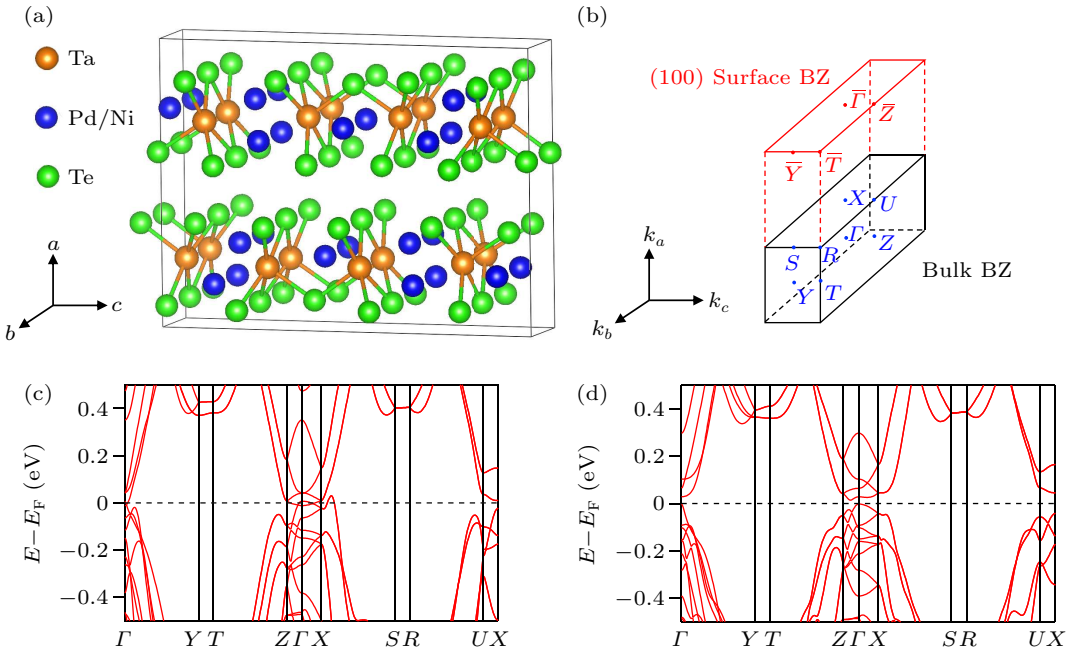


Fig. 1. Calculated band structure of $Ta_2Pd_3Te_5$ and $Ta_2Ni_3Te_5$. (a) Crystal structure of $Ta_2Pd_3Te_5$/$Ta_2Ni_3Te_5$. (b) Bulk and (100) surface Brillouin zone (BZ) of $Ta_2Pd_3Te_5$/$Ta_2Ni_3Te_5$. Calculated band structure of (c) $Ta_2Pd_3Te_5$ and (d) $Ta_2Ni_3Te_5$ along high-symmetry lines by DFT using the MBJ functional, respectively.

We then proceed to deposit potassium on the cleaved surface of $Ta_2Pd_3Te_5$ and $Ta_2Ni_3Te_5$. Considering that both VB and CB are observable under p polarization for $Ta_2Pd_3Te_5$, we choose p polarization as the experimental setup and set the temperature at 20 K to avoid the desorption of potassium adatoms from the sample surface. Figure 3 shows the evolution of the band structure of $Ta_2Pd_3Te_5$ at various surface potassium doping steps. At the very beginning, the CB is invisible due to the limited thermal broadening. After deposition of 2 min, the VB shifts downwards a little to higher binding energy and the CB bottom becomes observable, yet the band structure around $\bar{\Gamma}$ remains a gapped feature. Upon further deposition, the CB shifts downwards continuously and another electron band also appears above CB at a deposition time of 7 min. Moreover, the gap size at $\bar{\Gamma}$ is observably reduced compared to the doping step of 2 min (see Fig. 5(a) for compari-

son). We believe that the shift of VB and CB arises from three different reasons. First, the injection of excess electrons provided by alkali metal atoms leads to an upward shift in chemical potential, this will make both VB and CB shift downwards to higher binding energy. Second, excess charge carriers effectively enhance the screen effect of the Coulomb interactions and make the excitons unstable, leading to the reduction of the band gap. Lastly, the deposition of alkali metal atoms on the surface will introduce an extra electric field, making VB and CB shift in opposite energy directions to each other, known as the Stark effect.[5,33–37] Therefore, the shift of the CB and VB is not solely the effect of exciton instability, but the existence of the band gap still indicates the presence of remaining exciton condensation. After deposition of 9 min, the direct band gap at $\bar{\Gamma}$ is almost zero, and the dispersions around $\bar{\Gamma}$ change from parabolic to linear. Then at a deposition time of 11 min, the CB and VB cross each other, resulting in a semi-metallic band structure. This means that a metal–insulator phase transition occurs between 9 min and 11 min of deposition. The curvature intensity plots[38] of the ARPES data in Fig. 3(b) provide a clearer depiction of the evolution of the doping process. The red dashed line in the rightmost panel is the linear extrapolated CB, which indicates that the bottom of CB lies well under the top of CB. Our results further confirm the existence of spontaneous exciton condensation in $Ta_2Pd_3Te_5$ and demonstrate that $Ta_2Pd_3Te_5$ is sensitive to the concentration of charge carriers. Excess charge carriers provided by sufficient potassium dose successfully screen the Coulomb interactions between the parried electrons and holes and make the system recover to a normal semi-metallic state. It is also worth noting that the band overlap after potassium deposition for 11 min cannot reflect the real band overlap of the normal state of $Ta_2Pd_3Te_5$ due to the Stark effect.

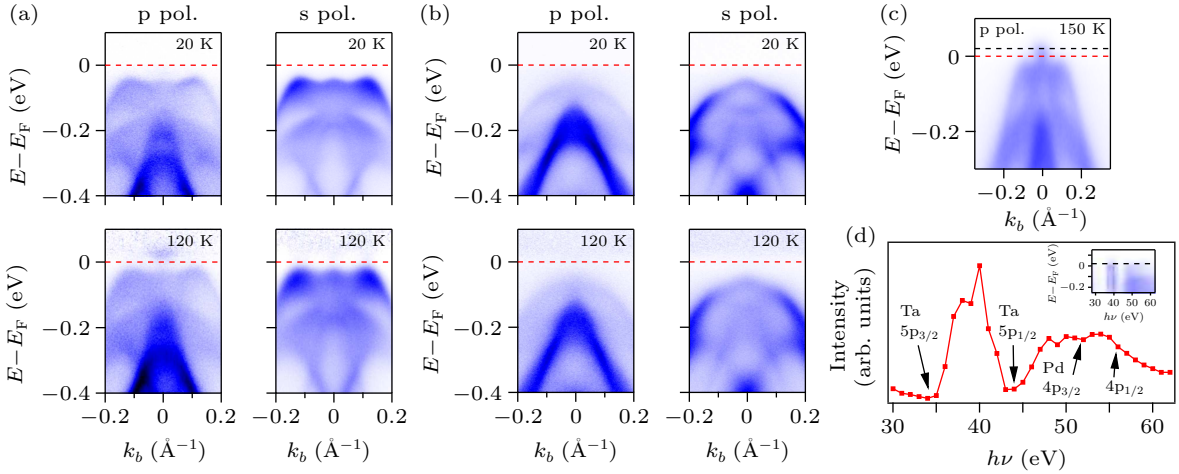


Fig. 2. ARPES spectrums under different experimental conditions. (a) Intensity plots of the ARPES data of $Ta_2Pd_3Te_5$ along $\bar{\Gamma}$–$\bar{Y}$ under p and s polarized lights at 20 K and 120 K. For clarity, the data at 120 K are divided by the Fermi–Dirac distribution function to visualize the CB bottom above E_F. (b) Similar to panel (a) but for $Ta_2Ni_3Te_5$. (c) Intensity plots of the synchrotron-based ARPES data of $Ta_2Pd_3Te_5$ along $\bar{\Gamma}$–$\bar{Y}$ with $h\nu = 25$ eV at 150 K. (d) $h\nu$ dependence of the spectral intensities at constant energy indicated by the black dashed lines in the inset and panel (c). Inset: intensity plot of the ARPES data at $\bar{\Gamma}$ with varying $h\nu$ at 150 K. The spectral intensities are normalized by photon flux.

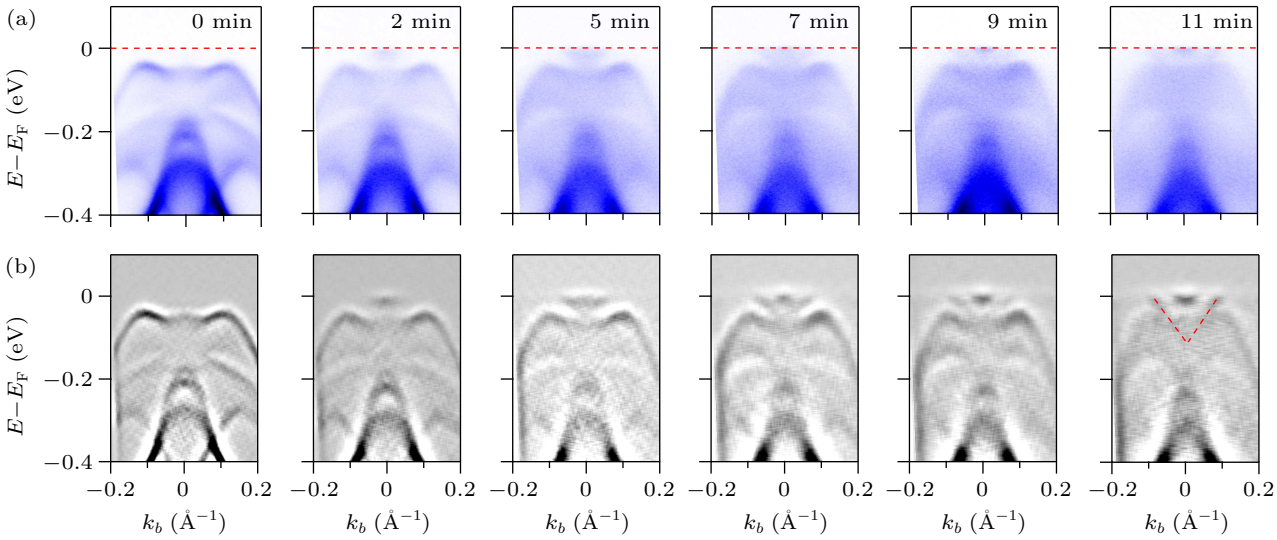


Fig. 3. Surface doping evolution of the band structure of $Ta_2Pd_3Te_5$. (a) Intensity plots of the ARPES data along $\bar{\Gamma}$–$\bar{Y}$ at different surface doping steps, all data were collected with p polarized laser at 20 K. (b) Curvature intensity plots of the data in panel (a).

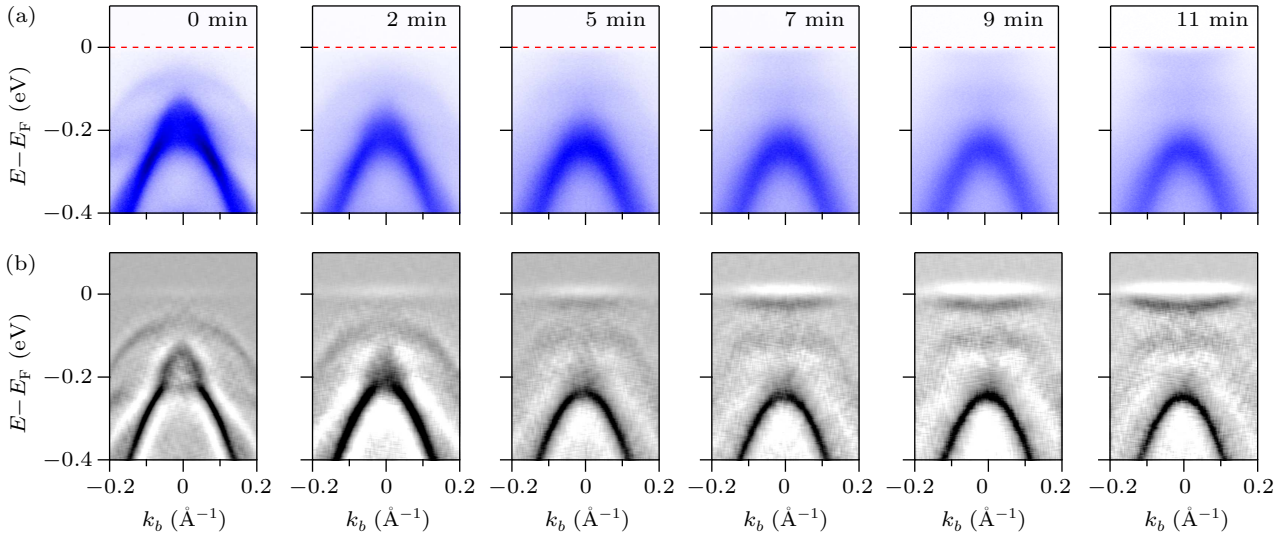


Fig. 4. Surface doping evolution of the band structure of $Ta_2Ni_3Te_5$ at different steps. (a) Intensity plots of the ARPES data along $\bar{\Gamma}$–$\bar{Y}$ at different surface doping steps, all data were collected with p polarized laser at 20 K. (b) Curvature intensity plots of the data in panel (a).

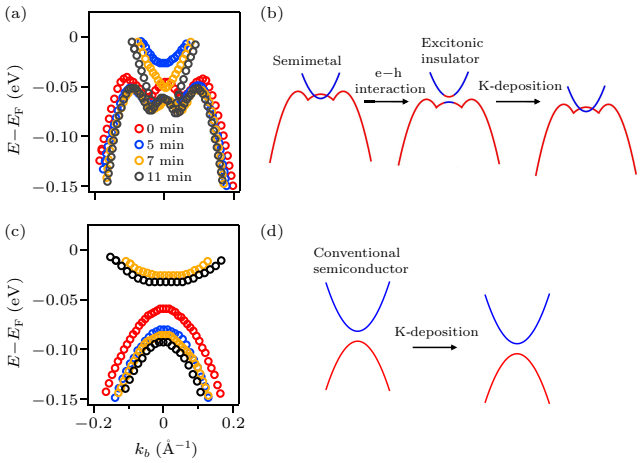


Fig. 5. Comparison of the band structure at different surface doping steps of $Ta_2Pd_3Te_5$ and $Ta_2Ni_3Te_5$. (a) Band dispersions of $Ta_2Pd_3Te_5$ determined by tracking the highest intensity values in Fig. 3(b) at different total deposition times. (b) Schematic diagram depicting how an excitonic phase can evolve from a normal semi-metallic state via electron–hole interactions, and then how to recover normal semi-metallic states via potassium deposition in $Ta_2Pd_3Te_5$. (c) Similar to panel (a), but for $Ta_2Ni_3Te_5$. (d) Schematic diagram depicting how the band structure of a conventional semiconductor in $Ta_2Ni_3Te_5$ evolves under potassium deposition.

As a comparison, Fig. 4 shows the evolution of the band structure of $Ta_2Ni_3Te_5$ at various surface potassium doping steps. The VB also shifts downwards to higher binding energy upon doping. In contrast to $Ta_2Pd_3Te_5$, the CB remains invisible at a deposition time of 2 min. After deposition of 5 min, there is finite spectral intensity around E_F, indicating the appearance of CB. The curvature intensity plots of the ARPES data in Fig. 4(b) provide a clearer view of the appearance of CB. We believe that the Stark effect plays a crucial role in the appearance of CB, since the Stark effect can reduce the gap between CB and VB in semiconductors, it helps make the CB observable together with the combined effect of the upward shift in chemical potential before 5 min. Upon further doping, both VB and CB continue shifting downwards, the band gap decreases but persists all the time. We attempt to deposit potassium on $Ta_2Ni_3Te_5$ for as long as 19 min, but it maintains an insulating state continuously. We believe that the distinct properties between $Ta_2Pd_3Te_5$ and $Ta_2Ni_3Te_5$ arise from the difference in band gap in their normal states. It is well known that EI usually occurs in semiconductors with small band gap or semimetals with small band overlap, where the binding energy of excitons exceeds the band gap or band overlap, but the band gap of $Ta_2Ni_3Te_5$ may be too large for excitons to form and condense spontaneously compared to $Ta_2Pd_3Te_5$, and this makes $Ta_2Ni_3Te_5$ a conventional semiconductor.

To better compare the band structure at different doping steps, we extract the band dispersion of $Ta_2Pd_3Te_5$ and $Ta_2Ni_3Te_5$ at several representative deposition times, as shown in Figs. 5(a) and 5(c). Colored circles are determined by tracking the highest intensity positions in the curvature intensity plots of the ARPES data in Figs. 3(b) and 4(b). For $Ta_2Pd_3Te_5$, the VB first shifts downwards to higher binding energy, then stays in almost the same energy position after a deposition time of 5 min. The CB of $Ta_2Pd_3Te_5$ shifts downwards continuously, resulting in markable reductions of the band gap at $\bar{\Gamma}$, and finally crosses with VB. It is also worth noting that the band dispersions around $\bar{\Gamma}$ change from parabolic to linear with increasing deposition time, this is very similar to the change of dispersion with increasing temperature. For $Ta_2Ni_3Te_5$, both CB and VB shift downwards continuously, and the band gap persists throughout all the deposition time. The shifts of VB and CB are almost same between 7 min and 11 min deposition, which shows only the effect of chemical potentialand the Stark effect is not crucial. Figure 5(b) illustrates the band evolution of $Ta_2Pd_3Te_5$: an EI state emerges from a normal semi-metallic state via inter-band electron–hole Coulomb interactions, then recovers to a normal semi-metallic state due to exciton instability after sufficient surface potas-

sium deposition, accompanied by the band shift resulting from chemical potential shift and the Stark effect. For $Ta_2Ni_3Te_5$ as a conventional semiconductor, Fig. 5(b) illustrates that there is only band shift without any phase transition throughout all the deposition time.

4. Conclusion and perspectives

We successfully induce a metal–insulator phase transition in $Ta_2Pd_3Te_5$ via surface alkali metal doping, accompanied by a transformation in the CB dispersions changing from parabolic to linear. However, the isostructural compound $Ta_2Ni_3Te_5$ shows no such phase transition under similar surface doping conditions. These results not only reinforce the identification of $Ta_2Pd_3Te_5$ as an EI, but also offer an effective method to manipulate the exotic quantum phenomenon, which can be used to design functional quantum devices.

Given that $Ta_2Pd_3Te_5$ and $Ta_2Ni_3Te_5$ share the same crystal structure, we propose that Ta_2 $(Pd_xNi_{1-x})_3Te_5$ $(0 < x < 1)$ samples with different x values can be grown to study how an EI evolves from conventional semiconductor. Besides, building on our previous studies, we have shown that the inter-band electron–hole Coulomb interactions in the EI phase disrupt the symmetry of the electronic state in $Ta_2Pd_3Te_5$, subsequently leading to a break of crystal symmetry via electron–lattice coupling.[28] Here we demonstrate that $Ta_2Pd_3Te_5$ could recover to normal semi-metallic phase via surface alkali metal doping, we propose further investigations using transmission electron microscopy (TEM) to examine changes in crystal symmetry post-doping. Such studies could provide deeper insights into the interplay between electronic states and crystal structure in these intriguing materials.

Acknowledgments

Project supported by the Ministry of Science and Technology of China (Grant No. 2022YFA1403800), the National Natural Science Foundation of China (Grant Nos. U2032204, 12188101, and U22A6005), the Chinese Academy of Sciences (Grant No. XDB33000000), the Synergetic Extreme Condition User Facility (SECUF), and the Center for Materials Genome.

References

[1] Mott N F 1961 *Philos. Mag.* **6** 287
[2] Halperin B I and Rice T M 1968 *Rev. Mod. Phys.* **40** 755
[3] Kohn W 1967 *Phys. Rev. Lett.* **19** 439
[4] Jérome D, Rice T M and Kohn W 1967 *Phys. Rev.* **158** 462
[5] Chen L, Han T T, Cai C, Wang Z G, Wang Y D, Xin Z M and Zhang Y 2020 *Phys. Rev. B* **102** 161116
[6] Monney C, Cercellier H, Battaglia C, Schwier E F, Didiot C, Garnier M G, Beck H and Aebi P 2009 *Physica B* **404** 3172
[7] Sun B S, Zhao W J, Palomaki T, Fei Z Y, Runburg E, Malinowski P, Huang X, Cenker J, Cui Y T, Chu J H, Xu X D, Ataei S S, Varsano D, Palummo M, Molinari E, Rontani M and Cobden D H 2022 *Nat. Phys.* **18** 94
[8] Tang T W, Wang H Y, Duan S F, Yang Y Y, Huang C Z, Guo Y F, Qian D and Zhang W T 2020 *Phys. Rev. B* **101** 235148
[9] Okazaki K, Ogawa Y, Suzuki T, Yamamoto T, Someya T, Michimae S, Watamabe M, Lu Y F, Nohara M, Takagi H, Katayama N, Sawa H, Fujisawa M, Kanai T, Ishii N, Itatani J, Mizokawa T and Shin S 2018 *Nat. Commun.* **9** 4322
[10] Wilson J A 1977 *Solid State Commun.* **22** 551
[11] Wilson J A 1978 *Phys. Status Solidi B* **86** 11
[12] Pillo T, Hayoz J, Berger H, Lévy F, Schlapbach L and Aebi P 2000 *Phys. Rev. B* **61** 16213
[13] Kidd T E, Miller T, Chou M Y and Chiang T C 2002 *Phys. Rev. Lett.* **88** 226402
[14] Cercellier H, Monney C, Clerc F, Battaglia C, Despont L, Garnier M G, Beck H, Aebi P, Patthey L, Berger H and Forró L 2007 *Phys. Rev. Lett.* **99** 146403
[15] Monney C, Schwier E F, Garnier M G, Mariotti N, Didiot C, Beck H, Aebi P, Cercellier H, Marcus J, Battaglia C, Berger H and Titov A N 2010 *Phys. Rev. B* **81** 155104
[16] Kogar A, Rak M S, Vig S, Husain A A, Flicker F, Joe Y I, Venema L, MacDougall G J, Chiang T C, Fradkin E, Wezel J V and Abbamonte P 2017 *Science* **358** 1314
[17] Wakisaka Y, Sudayama T, Takubo K, Mizokawa T, Arita M, Namatame H, Taniguchi M, Katayama N, Nohara M and Takagi H 2009 *Phys. Rev. Lett.* **103** 026402
[18] Kaneko T, Toriyama T, Konishi T and Ohta Y 2013 *Phys. Rev. B* **87** 035121
[19] Seki K, Wakisaka Y, Kaneko T, Toriyama T, Konishi T, Sudayama T, Saini N L, Arita M, Namatame H, Taniguchi M, Katayama N, Nohara M, Takagi H, Mizokawa T and Ohta Y 2014 *Phys. Rev. B* **90** 155116
[20] Larkin T I, Yaresko A N, Pröpper D, Kikoin K A, Lu Y F, Takayama T, Mathis Y L, Rost A W, Takagi H, Keimer B and Boris A V 2017 *Phys. Rev. B* **95** 195144
[21] Lu Y F, Kono H, Larkin T I, Rost A W, Takayama T, Boris A V, Keimer B and Takagi H 2017 *Nat. Commun.* **8** 14408
[22] Sugimoto K, Nishimoto S, Kaneko T and Ohta Y 2018 *Phys. Rev. Lett.* **120** 247602
[23] Fukutani K, Stania R, Kwon C I, Kim J S, Kong K J, Kim J and Yeom H W 2021 *Nat. Phys.* **17** 1024
[24] Zhao J F, Ou H W, Wu G, Xie B P, Zhang Y, Shen D W, Wei J, Yang L X, Dong J K, Arita M, Namatame H, Taniguchi M, Chen X H and Feng D L 2007 *Phys. Rev. Lett.* **99** 146401
[25] Fukutani K, Stania R, Jung J, Schwier E F, Shimada K, Kwon C I, Kim J S and Yeom H W 2019 *Phys. Rev. Lett.* **123** 206401
[26] Mitsuoka T, Suzuki T, Takagi H, Katayama N, Sawa H, Nohara M, Watanabe M, Xu J D, Ren Q H, Fujisawa M, Kanai T, Itatani J, Shin S, Okazaki K and Mizokawa T 2020 *J. Phys. Soc. Jpn.* **89** 124703
[27] Huang J R, Jiang B, Yao J Y, *et al.* 2024 *Phys. Rev. X* **14** 011046
[28] Zhang P, Dong Y Y, Yan D Y, *et al.* 2024 *Phys. Rev. X* **14** 011047
[29] Yao J Y, Sheng H H, Zhang R H, Pang R T, Zhou J J, Wu Q S, Weng H M, Dai X, Fang Z and Wang Z J 2024 arXiv: 2401.01222 [cond-mat.mtrl-sci]
[30] Guo Z P, Yan D Y, Sheng H H, Nie S M, Shi Y G and Wang Z J 2021 *Phys. Rev. B* **103** 115145
[31] Qian T, Xu N, Shi Y B, Nakayama K, Richard P, Kawahara T, Sato T, Takahashi T, Neupane M, Xu Y M, Wang X P, Xu G, Dai X, Fang Z, Cheng P, Wen H H and Ding H 2011 *Phys. Rev. B* **83** 140513
[32] Gao S Y, Zhang S, Wang C X, *et al.* 2023 *Phys. Rev. X* **13** 041049
[33] Khoo K H, Mazzoni M S C and Louie S G 2004 *Phys. Rev. B* **69** 201401
[34] Ishigami M, Sau J D, Aloni S, Cohen M L and Zettl A 2005 *Phys. Rev. Lett.* **94** 056804
[35] Ramasubramaniam A, Naveh D and Towe E 2011 *Phys. Rev. B* **84** 205325
[36] Kang M G, Kim B, Ryu S H, Jung S W, Kim J, Moreschini L, Jozwiak C, Rotenberg E, Bostwick A and Kim K S 2017 *Nano Lett.* **17** 1610
[37] Kim J, Balk S S, Ryu S H, Sohn Y, Park S, Park B G, Denlinger J, Yi Y, Choi H J and Kim K S 2015 *Science* **349** 723
[38] Zhang P, Richard P, Qian T, Xu Y M, Dai X and Ding H 2011 *Rev. Sci. Instrum.* **82** 043712